Ocean Systems Engineering, *Vol. 7, No. 3 (2017) 225-246*
DOI: https:// doi.org/10.12989/ose.2017.7.3.225

Suppression of tension variations in hydro-pneumatic riser tensioner by using force compensation control

Hooi-Siang Kang[1,2a], Moo-Hyun Kim*[3], Shankar S. Bhat Aramanadka[4b], Heon-Yong Kang[3c] and Kee-Quen Lee[5d]

[1]*Faculty of Mechanical Engineering, Universiti Teknologi Malaysia, Johor Bahru, Johor, Malaysia*
[2]*Institute for Vehicle Systems and Engineering (IVeSE), Universiti Teknologi Malaysia, Johor Bahru, Malaysia*
[3]*Department of Ocean Engineering, Texas A&M University, College Station, Texas, USA*
[4]*Sabah Shell Petroleum Co. Ltd., Kuala Lumpur, Malaysia*
[5]*Department of Mechanical Precision Engineering, Malaysia-Japan International Institute of Technology (MJIIT), Universiti Teknologi Malaysia Kuala Lumpur, Wilayah Persekutuan Kuala Lumpur, Malaysia*

(Received June 22, 2017, Revised August 28, 2017, Accepted August 30, 2017)

Abstract. Excessive dynamic-tension variations on the top-tensioned risers (TTRs) deteriorate the structural integrity and cause potential safety hazards. This phenomenon has become more remarkable in the development of deep-water fields with harsher environmental loads. The conventional prediction method of tension variations in hydro-pneumatic tensioner (HPT) has the disadvantage to underestimate the magnitude of cyclic loads. The actual excessive dynamic tension variations are larger when considering the viscous frictional fluid effects. In this paper, a suppression method of tension variations in HPT is modeled by incorporating the magneto-rheological (MR) damper and linear-force actuator. The mathematical models of the combined HPT and MR damper are developed and a force-control scheme is introduced to compensate the excessive tension variations on the riser tensioner ring. Numerical simulations and analyses are conducted to evaluate the suppression of tension variations in HPT under both regular- and irregular-wave conditions for a drilling riser of a tensioned-leg platform (TLP). The results show that significant reduction of tension variations can be achieved by introducing the proposed system. This research has provided a theoretical foundation for the HPT tension control and related structural protection.

Keywords: top-tensioned riser; hydro-pneumatic tensioner; tension variations; tension control; force compensation; magneto-rheological damper

1. Introduction

The safety of riser system for offshore oil and gas platforms is of critical importance for both structural integrity and environmental safety. Top-tensioned risers (TTRs) with dry-tree (well-head

*Corresponding author, Professor, E-mail: m-kim3@tamu.edu
[a] Ph.D., E-mail: kanghs@utm.my
[b] Ph.D., E-mail: Shankar.Bhat@shell.com
[c] Ph.D., E-mail: ga0prodg@tamu.edu
[d] Ph.D., E-mail: lkquen@utm.my

 ISSN: 2093-6702 (Print), 2093-677X (Online)

on deck) units are usually supported by hydro-pneumatic tensioner (HPT) systems. Conventionally, the analysis of TTR is based on a parametric formulation (Yang 2009) and the tension variations are caused by the relative displacement between the floating platform and the HPT. However, if the viscous effects of frictional fluid inside the HPT are considered (Kozik 1975, Kozik and Noerager 1976, Sten *et al.* 2010, Gallagher *et al.* 2012, Kang *et al.* 2017), the resulting tension variations can be larger, which can be an issue for fatigue estimation (Trent 2012, Gallagher *et al.* 2012). Kang *et al.* (2017) formulated the dynamic tension variations acting on the TTR by considering both frictional fluid and pneumatic effects and found that the excessive tension variations are notably induced from the fluid flow inside the HPT and its hoses. They are also affected by the geometrical dimension of hydraulic pipes and the volume of the gas tank. The tension variations on the tensioner ring can prompt detrimental effects to the structural integrity of the system by increasing the cyclic loads causing component fatigue. The dynamic tension variations also reduce the controllability of riser, especially during the drilling process.

Advanced materials can be employed to improve the overall TTR performance. Dominguez *et al.* (2008) reported that magneto-rheological (MR) dampers can modify their mechanical properties, such as stiffness and damping, by using rheological fluids and electric current. One unique advantage of the MR damper is that its damping characteristics can adaptively be altered by varying magnetic field (Spencer *et al.* 1997, Tse and Chang 2002). When rheological fluid is in the fluid state, the MR damper acts like a normal damper with un-magnetized condition. On the other hand, if the rheological fluid is magnetized by an electromagnetic field, the fluid particles are rearranged into a semi-solid state, which has higher resistance force. Their mechanical simplicity, high dynamic range, lower power requirements, large force capacity, robustness, and safety tolerance have made them an attractive device for semi-active control in civil, aerospace, and automotive applications (Dominguez *et al.* 2008). The MR-damper technology has also been successfully applied to minimizing structural vibration during the earthquake (Hurlebaus and Gaul 2006, Kim 2007, Osbulut *et al.* 2011) and the response reduction on bridges (Duan *et al.* 2002, Yang *et al.* 2011).

In this paper, the incorporation of MR damper into a HPT system to reduce the dynamic tension variations is investigated. The objectives of this paper are: (i) to derive the mathematical model of the combined effects of HPT and MR damper; (ii) to develop a control scheme for compensating the excessive tension variations; and (iii) to numerically analyze the suppression of tension variations in HPT in the proposed system.

2. Methodology

2.1 Modeling of hydro-pneumatic tensioner

A direct-acting tensioner (DAT), as shown in Fig. 1, can be modeled as a hydro-pneumatic system. The industrial practices normally assume that the frictional losses of hydraulic oil between the accumulator and the tensioner cylinder are to be neglected (Yang 2009). Therefore, the force equilibrium of tensioner F_{ten} according to parametric formulation can be represented as

$$F_{ten} = F_{HP_0}^{a}\left(1-\frac{\Delta z}{z_{A0}}\right)^{-\gamma} \tag{1}$$

where $F_{HP0}{}^{a}$ is the initial force acting on the piston at the piston-side, Δz is the change of platform-riser relative displacement, z_{A0} is the total equivalent length of cylinder stroke in piston-side, γ is adiabatic gas constant, which is 1.4 for nitrogen at 15°C (Li *et al.* 2013). The parametric formulation in Eq. (1) is reasonably accurate if the total length of connection pipes is sufficiently short (Trent 2012) or the relative velocity of the platform-riser in the heave direction is sufficiently small, such as in the case of the tensioned-leg platform (TLP). However, it is noteworthy that the hydraulic pressure losses through the pipes between the accumulator and the piston in Fig. 1 must be evaluated if the velocity of riser stroke is sufficiently large, such as under the operations of the drillship, dry-tree semisubmersible, and during the anti-recoiling and disconnection of TTR. By considering the existence of fluid friction in the accumulator, the pressure variations can have a range from few bars to over 100 bars (Grønevik 2013). The force equilibrium on both sides of tensioner piston F_{ten} in the hydraulic-pneumatic cylinder can be modified as (Kang *et al.* 2017)

$$F_{ten} = F_{HP_0}^{a}\left(1-\frac{\Delta z}{z_{A0}}\right)^{-\gamma} + A_p^{a}\cdot\frac{\rho_{oil} f^{AP}}{2A_{AP}^{2}}\left(\frac{L^{AP}+L_{eq}^{AP}}{D_{AP}}\right)q_{oil}\cdot\left|q_{oil}\right| - F_{HP_0}^{b}\left(1+\frac{\Delta z}{z_{B0}}\right)^{-\gamma} + F_{HS} \tag{2}$$

where $A_p{}^{a}$ is the cross sectional area of the piston at the piston-side, ρ_{oil} is the density of hydraulic oil, q_{oil} is the flow rate of hydraulic oil, f^{AP}, A_{AP}, and D_{AP} are the friction factor, cross sectional area, and diameter of the pipe from the accumulator (superscript A) to the tensioner piston (superscript P), respectively. L^{AP} is the geometrical length and $L_{eq}{}^{AP}$ is the equivalent lengths to account for local resistances, such as bends, fittings, inlet and outlet losses, and so on, from the accumulator (superscript A) to the tensioner piston (superscript P). $F_{HP0}{}^{b}$ is the initial force acting on the piston at the cap-side, z_{B0} is the total equivalent length of cylinder stroke in cap-side, and F_{HS} is the hard-stop force when the piston is approaching very closely to the upper/lower limits of the cylinder, which can be modeled as a cubic spring force (Yang 2009).

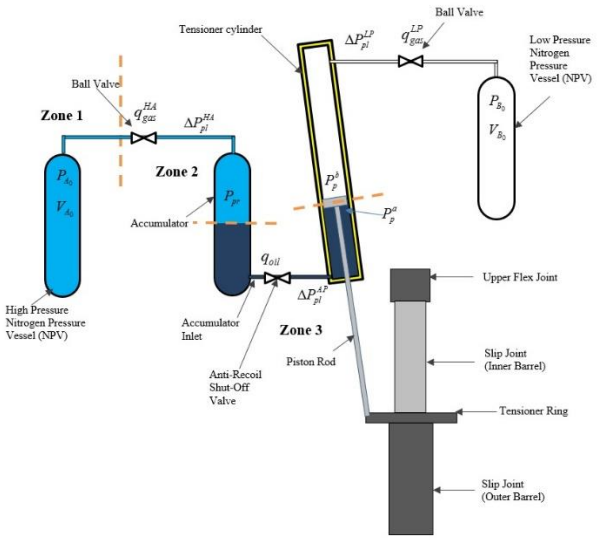

Fig. 1 Schematic diagram of direct-acting tensioner (DAT) system (Kang *et al.* 2017)

2.2 Modeling of magneto-rheological damper

A magneto-rheological (MR) damper (Spencer *et al.* 1997, Yang *et al.* 2004, Friedman *et al.* 2012), as shown in Fig. 2, is a device that employs rheological fluids to modify its mechanical properties. The stiffness and damping of the MR damper change when exposed to magnetic-field change (Dominguez *et al.* 2008). It has the advantages of mechanical simplicity, high dynamic range, lower power requirements, large-force capacity, robustness, and safe failure modes.

The Nonlinear Hysteretic Arctangent Function (NHAF) Model (Yang *et al.* 2011) is employed to model the nonlinear hysteretic model of MR damper. This hysteresis model possesses an appealing mathematical simplicity and is able to represent a large class of hysteretic behaviors and inelastic stress-strain relationships. The force exerted by the MR damper f_{MR} can be represented by the following equation

$$f_{MR} = c_{MR}\dot{x}_{MR} + k_{MR}x_{MR} + \alpha z_{MR} \tag{3}$$

$$z_{MR} = \tan^{-1}\left(\beta\dot{x}_{MR} + \delta\,\mathrm{sgn}\left(x_{MR}\right)\right) \tag{4}$$

where c_{MR} is the viscous damping coefficient of the MR damper, k_{MR} is the stiffness coefficient of the MR damper, x_{MR} and $\dot{x}_{MR}$ are the displacement and velocity of the piston of the MR damper, respectively. The hysteretic behavior of MR damper is expressed by the adjustable shape variables of the hysteresis loops; α, β, and δ. These variables can control the linearity in the unloading and the smoothness of the transition from the pre-yield to the post-yield region. The model variables of the MR damper governing equation c, k, α, β, and δ are functions of the applied command electric current i as proposed by Yang *et al.* (2011). By grouping $\mathbf{H} = [c, k, \alpha, \beta, \delta]$, then these variables, as listed in Table 1 can be fine-tuned with respect to electric current i as

$$\mathbf{H} = H_2 i^2 + H_1 i^1 + H_0 \tag{5}$$

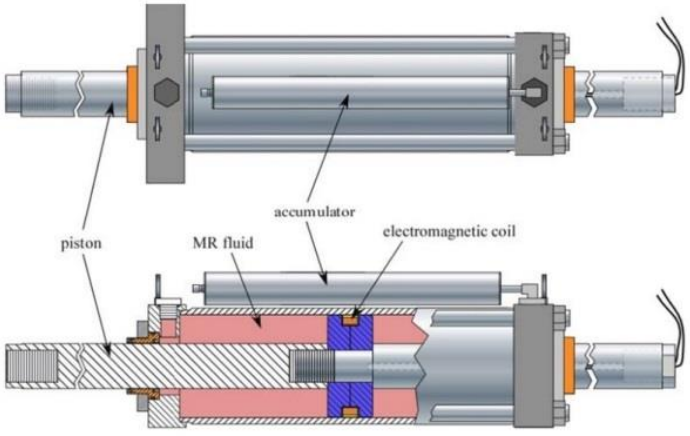

Fig. 2 Configuration of MR damper (Friedman *et al.* 2012)

Table 1 Adjustable shape variables of the MR damper hysteresis loops (Kang 2015)

	H_1	H_2	H_3
c_{MR}	8.5×10^5	1.44×10^8	6.0×10^6
k_{MR}	0	1.2×10^5	9.8×10^3
α	2.571×10^6	4.11×10^6	8.0×10^4
β	0	22.05	17.82
δ	0	2.6	2.3

The force-displacement and force-velocity loops with respect to different command electric current inputs i generated by the NHAF model and Kang (2015) are depicted in Figs. 3-5. The characteristics of these figures are: (i) the damping force increases with respect to the increment of command current i, excitation amplitude A, and excitation frequency ω, and it approaches a limiting value when the current gets a certain value; (ii) the ratio of the maximum damping force from 0 A to 0.4 A is about 2.5 times, which indicates that the adjustability of the damping force is preferable (Yang *et al.* 2011); (iii) the force-displacement loops are close to an elliptical shape, and the force-velocity loops are nonlinear hysteretic, which demonstrates that the energy dissipation ability of the damper is adequate (Yang *et al.* 2011). It is noteworthy that the frictional lagging effect is not represented in the force-velocity plot based on the selection of fine-tuned coefficients employed in this NHAF model in order to simplify this model.

2.3 Integration of hydro-pneumatic tensioner with magneto-rheological damper

In a conceptual set-up to suppress the tension variations in a hydro-pneumatic tensioner, the MR damper is assumed to be ideally attached to the tensioner ring and production deck as shown in Fig. 6.

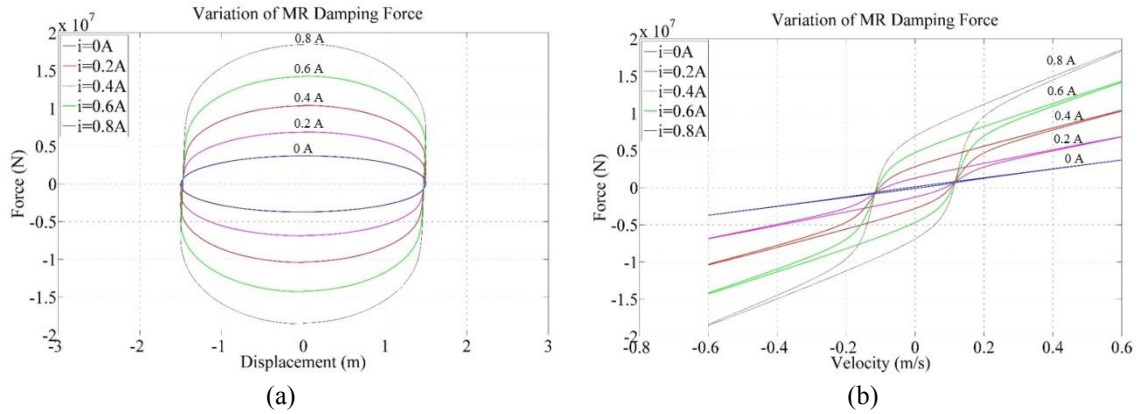

(a) (b)

Fig. 3 Damping force with respect to input currents, (a) force-displacement curves, and (b) force-velocity curves, with sinusoidal excitation amplitude = 1.5 m and sinusoidal excitation frequency = 0.4 rad/s

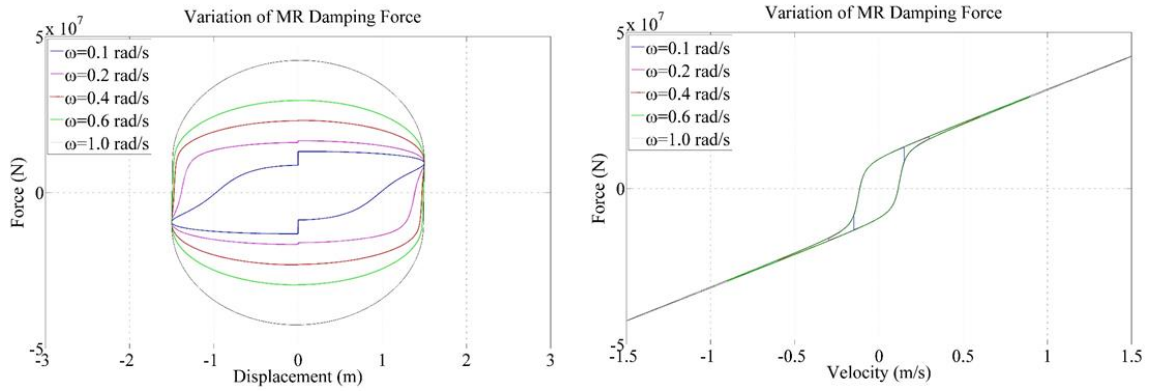

(a) (b)

Fig. 4 Damping force with respect to excitation frequency, (a) force-displacement curves, and (b) force-velocity curves, with sinusoidal excitation amplitude = 1.5 m and input current = 1.0 A

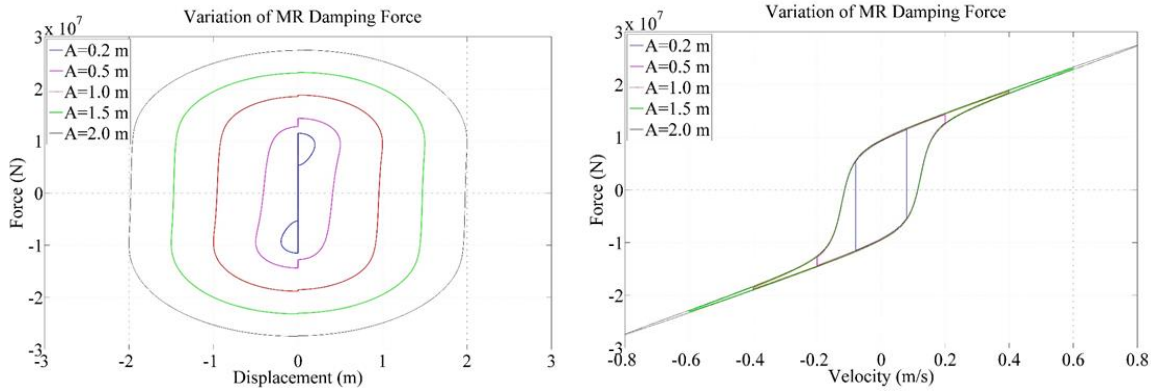

(a) (b)

Fig. 5 Damping force with respect to excitation amplitude, (a) force-displacement curves, and (b) force-velocity curves, with sinusoidal excitation frequency = 0.4 rad/s and input current = 1.0 A

This arrangement can be modeled as a lumped mass-spring-damper (MSD) system, as shown in Fig. 7, where the mass of host platform m_1 and tensioner m_2 are lumped, and the stiffness k_t and damping c_t of the tensioner are modeled as a spring and a dashpot, respectively. This model was assumed here to be in the vertical movement only while the rotations are assumed to be negligible.

The MR damper works corporately with the tensioner in order to reduce the required stroke on the tensioner with the trade-off of local tension increment. By referring to the free-body diagram in Fig. 7, the output force of MR damper in Eqs. (3) and (4) can be rewritten as

$$f_{MR}\big|_{x_1-x_2} = c_{MR}\left(\dot{x}_1-\dot{x}_2\right)+k_{MR}\left(x_1-x_2\right)+\alpha z_{(\dot{x}_1-\dot{x}_2)} \tag{6}$$

$$z_{(\dot{x}_1-\dot{x}_2)} = \tan^{-1}\left(\beta\left(\dot{x}_1-\dot{x}_2\right)+\delta\,\mathrm{sgn}\left(x_1-x_2\right)\right) \tag{7}$$

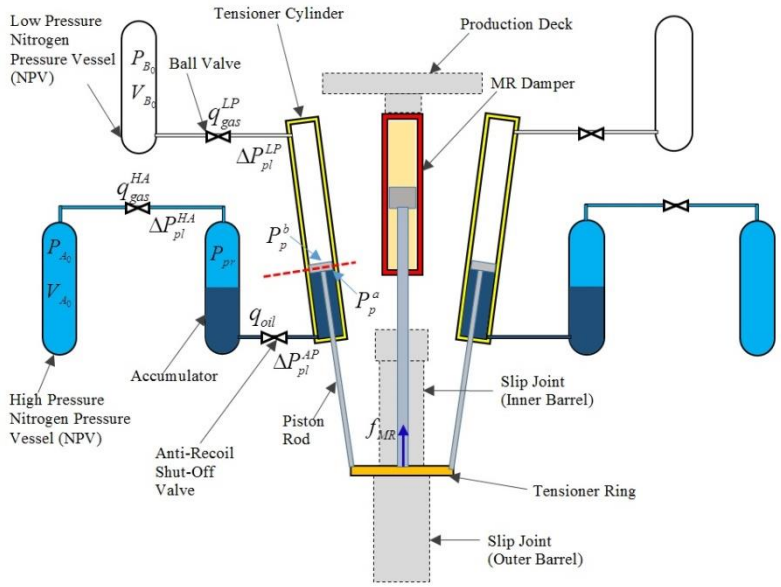

Fig. 6 The integration of MR damper in the HPT system

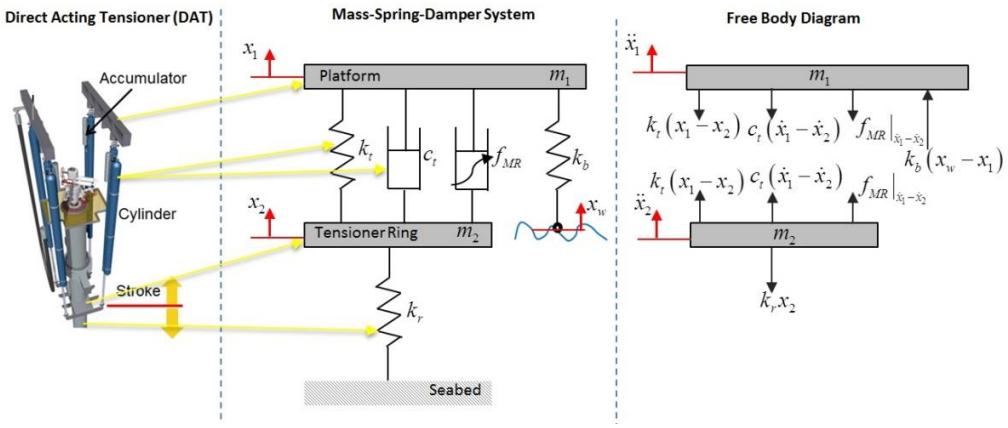

Fig. 7 Schematic diagram and free-body diagram for mass-spring-damper (MSD) system of direct-acting style tensioner (DAT) equipped with MR damper

where x_1 is the displacement of the host platform, x_2 is the displacement of tensioner ring, and $(\cdot)$ is the time derivative. The equations of motion for DAT equipped with MR damper in this 2-DOF model (Yao *et al.* 2002) are represented as

$$\begin{cases} m_1\ddot{x}_1 - \left(k_t + k_{MR}\right)\left(x_2 - x_1\right) - \left(c_t + c_{MR}\right)\left(\dot{x}_2 - \dot{x}_1\right) + k_b\left(x_1 - x_w\right) = \alpha z_{\left(\dot{x}_2 - \dot{x}_1\right)} \\ m_2\ddot{x}_2 + \left(k_t + k_{MR}\right)\left(x_2 - x_1\right) + \left(c_t + c_{MR}\right)\left(\dot{x}_2 - \dot{x}_1\right) + k_r x_2 = -\alpha z_{\left(\dot{x}_2 - \dot{x}_1\right)} \end{cases} \tag{8}$$

where k_b is the stiffness of the host platform body, k_r is the stiffness of the riser, and x_w refers to the displacement of wave amplitude in the vertical direction.

The finite element (FE) model of the HPT and the floating platform motion is developed in CHARM3D, a fully-coupled time-domain dynamic-analysis program for floating bodies, mooring lines/tendons, and risers (Ran 2000; Koo *et al.* 2004; Yang and Kim 2011; Kang and Kim 2012; Bae and Kim 2013; Kang *et al.* 2013; Kang *et al.* 2014; Kim and Kim 2015). The frequency-dependent hydrodynamic coefficients and the first-order and second-order wave excitation forces and moments are calculated by the near-field method by using WAMIT (Lee and Newman 1991), a diffraction/radiation panel program. The corresponding wave forces are converted to the time-domain terms using a two-term Volterra series expansion in CHARM3D. The frequency-dependent radiation damping was included in the form of a convolution integral in the time domain simulation. Viscous forces are included through the drag force term in Morison's equation (Yang and Kim 2010). A detailed modeling of coupled dynamics of floating platform and riser in CHARM3D can be found in Ran (2000). The coupling terms of riser finite element tangential stiffness matrix that needs to be added into the global stiffness matrix in CHARM3D after including tension variations was discussed in Kang *et al.* (2017) as

$$\frac{\Delta t}{2}\left\{\begin{bmatrix} 0 & 0 & K_{ij}^{rX} & K_{ij}^{r\theta} \\ 0 & 0 & 0 & K_{ij}^{r'\theta} \\ K_{ij}^{Xr} & 0 & 0 & 0 \\ K_{ij}^{\theta r} & K_{ij}^{\theta r'} & 0 & 0 \end{bmatrix}_{LS} + \begin{bmatrix} 0 & 0 & K_{ij}^{rX} & K_{ij}^{r\theta} \\ 0 & 0 & 0 & 0 \\ K_{ij}^{Xr} & 0 & 0 & 0 \\ K_{ij}^{\theta r} & 0 & 0 & 0 \end{bmatrix}_{TV}\right\}\begin{Bmatrix} \Delta r_j \\ \Delta r_j' \\ \Delta X_j \\ \Delta \theta_j \end{Bmatrix} = \frac{\Delta t}{2}\begin{Bmatrix} 2N_i \\ 2L_i \\ 2F_i \\ 2M_i \end{Bmatrix} + \frac{\Delta t}{2}\begin{Bmatrix} -2\cdot n_{cyn}\cdot F_{HP_{dyn}} \\ 0 \\ 2\cdot n_{cyn}\cdot F_{HP_{dyn}} \\ 0 \end{Bmatrix}_{TV} \tag{9}$$

where K_{ij}^{AB} is the coupling stiffness coefficients. The symbol K_{ij}^{AB} indicates that the tangential stiffness coefficient for the degree of freedom *B* in the direction *A*. The subscript *LS* refers to the coupling connection between the floating platform and riser top node based on Eq. (1). On the other hand, the subscript *TV* refers to the addition of tension variations on the coupling connection. Δt is time step of the numerical simulation, ΔX_j is the change of translational motion of the floating platform at its origin of the body coordinate system at each simulation step and $\Delta\theta_j$ is the change of angular motion of the floating platform at each simulation step. Also, Δr_j is the change of position of the riser top node which is connected to the floating platform and $\Delta r_j'$ is the change of tangent to the riser centerline at each simulation step. N_i is the nodal resultant force on the riser top node, F_i is the nodal resultant force acting on the floating platform, where F_i=-N_i. Moreover, L_i is the nodal resultant moment on the riser top node, and M_i is the nodal resultant moment acting on the floating platform, where $M_i = L_i \times r_i'$ (Ran 2000). n_{cyn} is the total number of the hydro-pneumatic cylinder of the riser tensioner, and F_{HPdyn} is the dynamic term which causes the frictional effects in the tensioner (Kang *et al.* 2017).

After taking the suppression force from MR damper in Eqs. (6)-(8) into Eq. (9), the coupling terms of riser finite element tangential stiffness matrix that needs to be added into the global stiffness matrix in CHARM3D is represented as

$$\frac{\Delta t}{2}\left\{\begin{bmatrix} 0 & 0 & K_{ij}^{rX} & K_{ij}^{r\theta} \\ 0 & 0 & 0 & K_{ij}^{r'\theta} \\ K_{ij}^{Xr} & 0 & 0 & 0 \\ K_{ij}^{\theta r} & K_{ij}^{\theta r'} & 0 & 0 \end{bmatrix}_{LS} + \begin{bmatrix} 0 & 0 & K_{ij}^{rX} & K_{ij}^{r\theta} \\ 0 & 0 & 0 & 0 \\ K_{ij}^{Xr} & 0 & 0 & 0 \\ K_{ij}^{\theta r} & 0 & 0 & 0 \end{bmatrix}_{TV}\right\}\begin{Bmatrix} \Delta r_j \\ \Delta r_j' \\ \Delta X_j \\ \Delta \theta_j \end{Bmatrix} = \frac{\Delta t}{2}\begin{Bmatrix} 2N_i \\ 2L_i \\ 2F_i \\ 2M_i \end{Bmatrix} + \frac{\Delta t}{2}\begin{Bmatrix} -2\cdot n_{cyn}\cdot F_{HP_{dyn}} \\ 0 \\ 2\cdot n_{cyn}\cdot F_{HP_{dyn}} \\ 0 \end{Bmatrix}_{TV} + \frac{\Delta t}{2}\begin{Bmatrix} 2f_{MR} - 2(c_{MR}+\gamma)\left(\dot{r}_j\right) \\ 0 \\ -2f_{MR} + 2(c_{MR}+\gamma)\left(\dot{X}_j\right) \\ 0 \end{Bmatrix}_{MR} \tag{10}$$

where

$$\gamma = \frac{\alpha\beta}{\left[\beta\left(\dot{X}_i + \dot{\theta}_j C_{ji} - \dot{r}_i\right) \pm \delta\right]^2 + 1} \tag{11}$$

where X_j and θ_j are the translational motion and angular motion, respectively, of the floating platform at its origin of the body coordinate system at each simulation step, r_j is the position of the riser top node which is connected to the floating platform, and C_{ji} is an 3×3 matrix to determine the orientation of angular motion. The details of derivation for the coupling terms as stated in Eq. (10) can be found in Kang (2015).

2.4 Modeling of Equivalent Force Compensation Control (EFCC)

A conceptual control scheme, named as the Equivalent Force Compensation Control (EFCC), to reduce the tension variations in between the actual TTR tension and the desired tension by using a combination of MR dampers and force actuators was discussed in this section. The conceptual system and design principle of EFCC are shown in Fig. 8. This setting was modified from Fig. 6 by adding two pairs of MR damper and force actuator, which are working in the opposite direction with each other. A force actuator provides constant force F_{CA} in the same direction of tensioner ring displacement. The actuator force F_{CA} can be regarded as an additional nodal resultant force on the riser top node N_i and on the floating platform F_i in the global stiffness matrix as stated in Eq. (10).

The MR damper, on the other hand, provides tunable resistive force f_{MR} in the counter-direction of tensioner ring displacement. The actuator force F_{CA} is then to be fine-tuned by adding the MR damper force f_{MR} in the opposite direction to produce a net force on the tensioner ring. The total force acting on the tensioner ring F_{TR} can be represented as

$$F_{TR} = F_{ten} + F_{MR} + F_{CA} \tag{12}$$

where F_{ten} is the equilibrium force on the tensioner piston in the hydraulic-pneumatic cylinder. F_{MR} refers to the combined force of both primary and secondary MR dampers in the conceptual setting as illustrated in Fig. 8. The primary MR damper is referred to the one moving in the same direction with the tensioner ring, and the secondary MR damper is the one acting in the opposite direction with respect to the motion of tensioner ring. Therefore, an MR damper swapping its role as the primary and secondary damper with respect to the tensioner ring motion, in back and forth. The MR

damper force is designed to compensate the dynamic axial tension variations exerted on the tensioner ring, as stated in the second terms on the right-hand-side of Eq. (2), by the HP tensioner with respect to the given displacement *z* and velocity *dz/dt*. The principle of force control scheme for EFCC, as shown in Fig. 8(b), indicates that the required combined MR damper output force to compensate the tension variations for each time step is calculated as (Kang 2015)

$$F_{MR} = F_{MR}^{P}\big|_{i=X} + \mathrm{sgn}(F_{req}) \cdot \left| \left(F_{MR}^{S}\big|_{i=0} \right) \right| \tag{13}$$

where $F_{MR}{}^{P}|_{i=X}$ refers to the primary MR damper force under the command current $i = i(X)$, and $F_{MR}{}^{S}|_{i=0}$ is the secondary MR damper force with the command current $i = 0$ A. The required force F_{req} to be generated by the combination of MR dampers is defined as

$$F_{req} = \begin{cases} -F_{ten} + T_{pr} + F_{CA} & \text{if } F_{ten} - T_{pr} \geq 0 \\ -F_{ten} + T_{pr} - F_{CA} & \text{if } F_{ten} - T_{pr} < 0 \end{cases} \tag{14}$$

where T_{pr} is the pretension (also regarded as the targeted tension in our case) of the DAT system.

The command electric current *i(X)* for the primary MR damper is calculated as

$$i(X) = \begin{cases} i_L^P = i\big|_{i=\mathrm{mid}}; \quad i_U^P = i\big|_{i=\max}; \quad i_C^P = \left(i_L^P + i_U^P\right)/2 & \text{if } F_{MR} < F_{req} \\ i_L^P = i\big|_{i=\min}; \quad i_U^P = i\big|_{i=\mathrm{mid}}; \quad i_C^P = \left(i_L^P + i_U^P\right)/2 & \text{if } F_{MR} \geq F_{req} \end{cases} \tag{15}$$

where $i_L{}^P$, $i_U{}^P$, and $i_C{}^P$ refer to the lowest electric current limit, highest electric current limit, and control electric current of the primary MR damper, respectively. The $i|_{i=min}$, $i|_{i=max}$, and $i|_{i=mid}$ denote the minimum current input (less than 0.001 A), maximum current input (3.0 A), and mid-point of these two current inputs, respectively. In this study, the targeting MR damper force F_{MR} in Eq. (13) is iterated until its deviation from the required force F_{req} is less than two-percent.

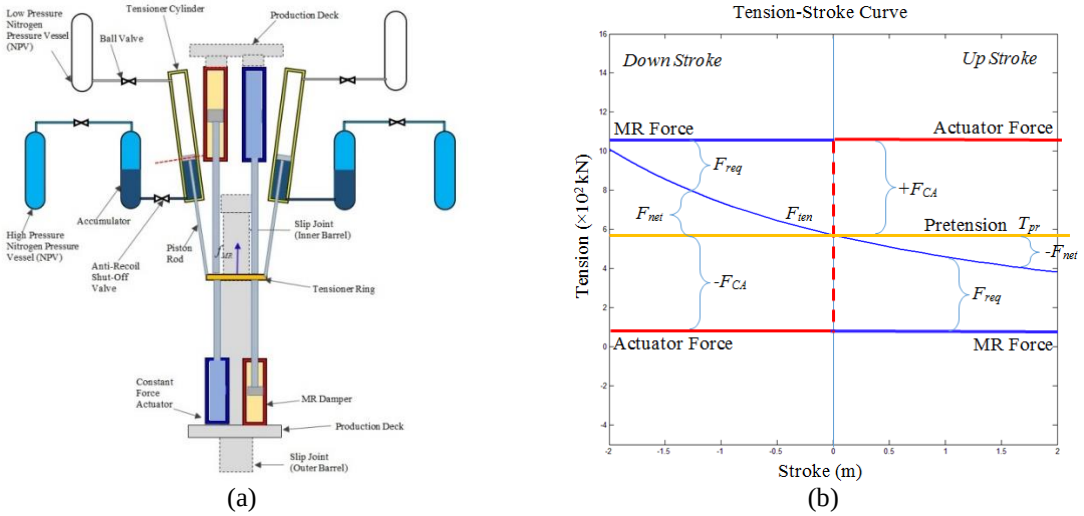

Fig. 8 Equivalent force compensation control (EFCC), (a) MR dampers and force actuators in the direct acting tensioner system and (b) Control principle

3. Numerical analyses on sensitivity of MR damper

Since the MR damper force in the EFCC is utilized to fine-tune the required tension on the tensioner ring, therefore, a large output force is not required. The coefficients of MR damper are modified from Table 1 into the values as tabulated in Table 2 in the simulation. The capacity of this MR damper based on the proposed variables in Table 2 is up to ~150 kN (~33.7 kips) when it acts at the displacement amplitude of 1.0 m (3.28 ft), with excitation frequency at 0.6 rad/s, and initial piston position offset at -17.0 m (-55.77 ft). The variations of MR damper forces under different combinations of amplitudes, frequencies, and controlled currents are shown in Figs. 9-14. The initial piston position offset is referred to the adjustment of the nominal position of MR damper with respect to the mean displacement of the tensioner ring in the particular cases.

The sensitivity of MR damper force with respect to the excitation frequency can be observed from Figs. 9 and 10. At a higher excitation frequency, the velocity $\dot{x}_{MR}$ is also higher so that the force of MR damper f_{MR}, as defined in Eq. (3), can be fully developed into a larger hysteresis loop as shown in Fig. 9. It can be observed that when the MR damper is excited under slower velocity, for instance, 0.08 rad/s as shown in the Fig. 10, the exerted force of MR damper is smaller.

On the other hand, the sensitivity of initial piston position of MR damper is shown in Figs. 11-14, for the initial piston positions for -17 m, +17 m, +19 m, and +12 m, respectively. The behaviors of MR damper with different initial piston positions must be identified because the ratio of the maximum damping force from 0 A to 3.0 A is varying with respect to the initial piston position. The tension-displacement loops are no longer symmetry in Figs. 11-14 during the tension/compression cycle. This phenomenon can be adequately explained by Eq. (3) where the term $k_{MR} \cdot x_{MR}$ has an initial tension/compression when an initial piston position is applied. The asymmetry characteristic of MR damper due to initial piston position is important for the design of riser system in determining the optimum position of MR damper compensating force.

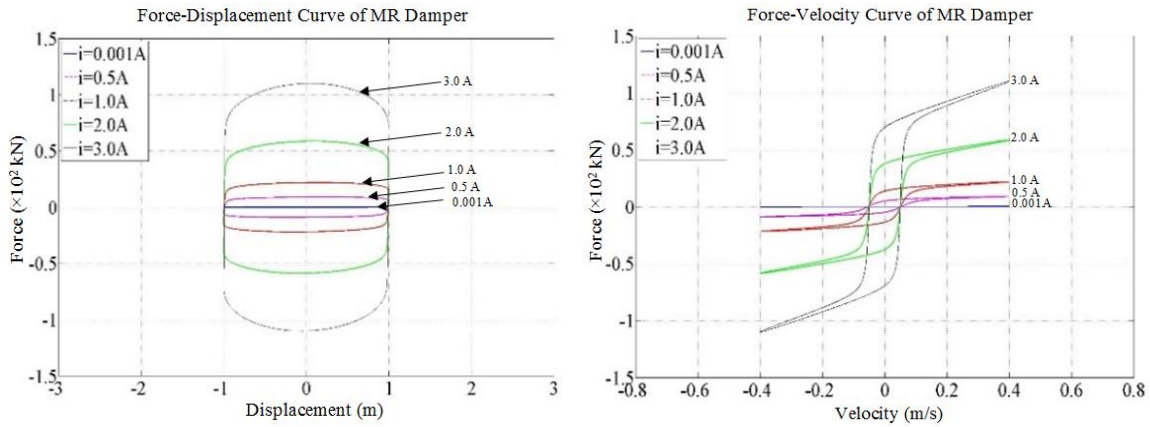

(a) (b)

Fig. 9 Variation of damping force with input currents, (a) force-displacement curves, and (b) force-velocity curves; with sinusoidal excitation amplitude = 1.0 m and sinusoidal excitation frequency = 0.6 rad/s

Table 2 Adjustable shape variables of the MR damper hysteresis loops (Kang 2015)

	H_1	H_2	H_3
c_{MR}	8500	5400	50
k_{MR}	0	540	50
α	2500	8100	40
β	0	52.05	2.82
δ	0	2.6	0.25

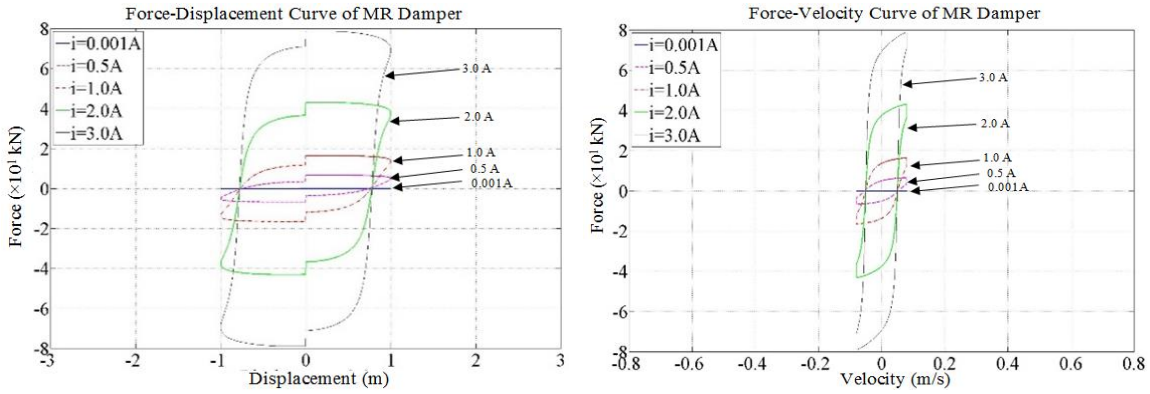

(a) (b)

Fig. 10 Variation of damping force with input currents, (a) force-displacement curves, and (b) force-velocity curves; with sinusoidal excitation amplitude = 1.0 m and sinusoidal excitation frequency = 0.08 rad/s

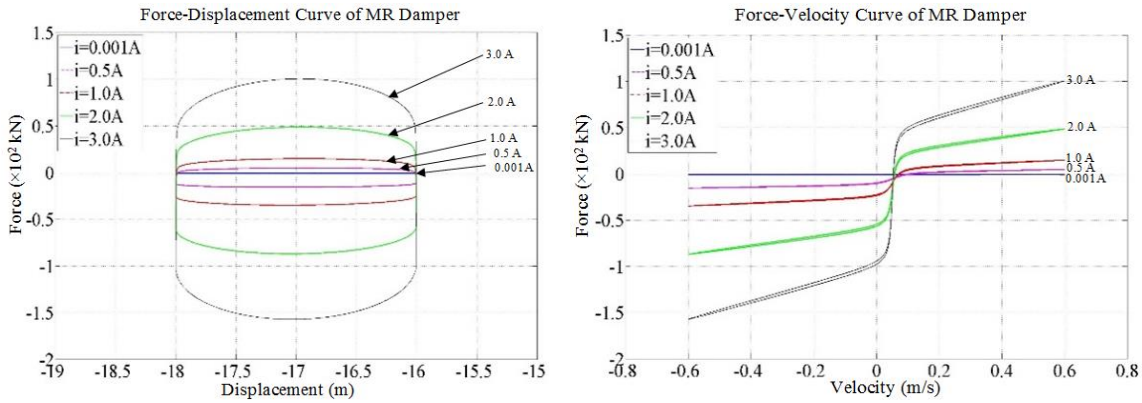

(a) (b)

Fig. 11 Variation of damping force at primary MR damper with input currents, (a) force-displacement curves, and (b) force-velocity curves; with sinusoidal excitation amplitude = 1.0 m and sinusoidal excitation frequency = 0.6 rad/s, initial piston position offset = -17.0 m (-55.77 ft)

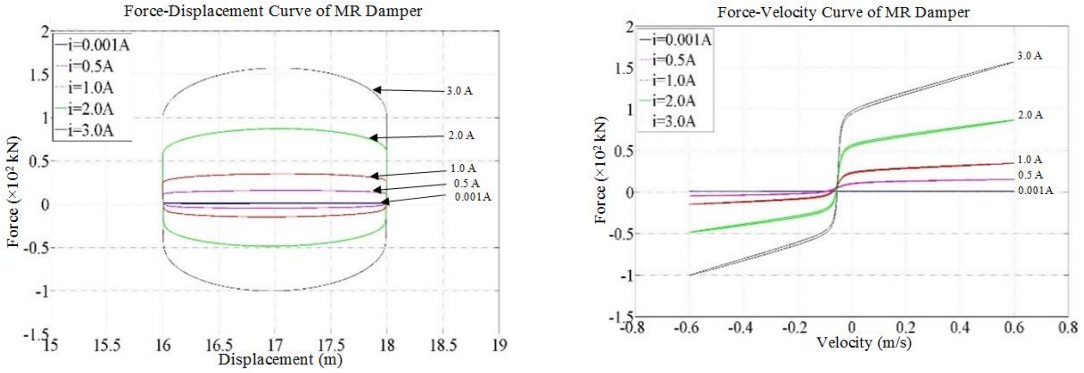

(a) (b)

Fig. 12 Variation of damping force at primary MR damper with input currents, (a) force-displacement curves, and (b) force-velocity curves; with sinusoidal excitation amplitude = 1.0 m and sinusoidal excitation frequency = 0.6 rad/s, initial piston position offset = +17.0 m (+55.77 ft)

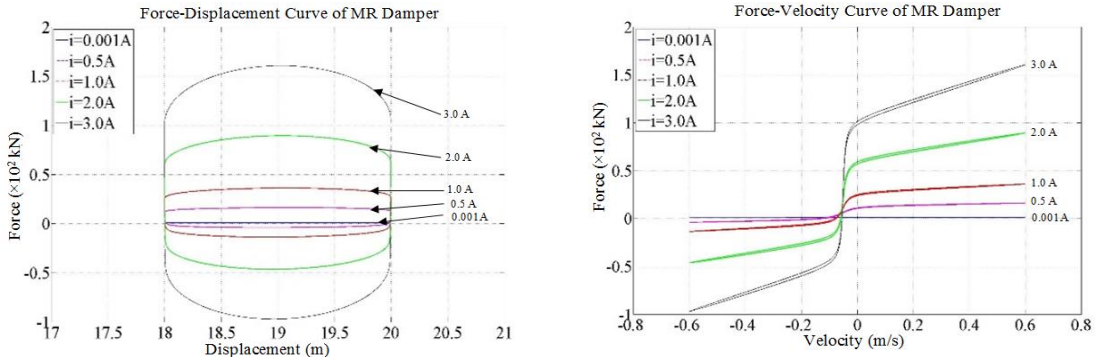

(a) (b)

Fig. 13 Variation of damping force at primary MR damper with input currents, (a) force-displacement curves, and (b) force-velocity curves; with sinusoidal excitation amplitude = 1.0 m and sinusoidal excitation frequency = 0.6 rad/s, initial piston position offset = +19.0 m (+62.34 ft)

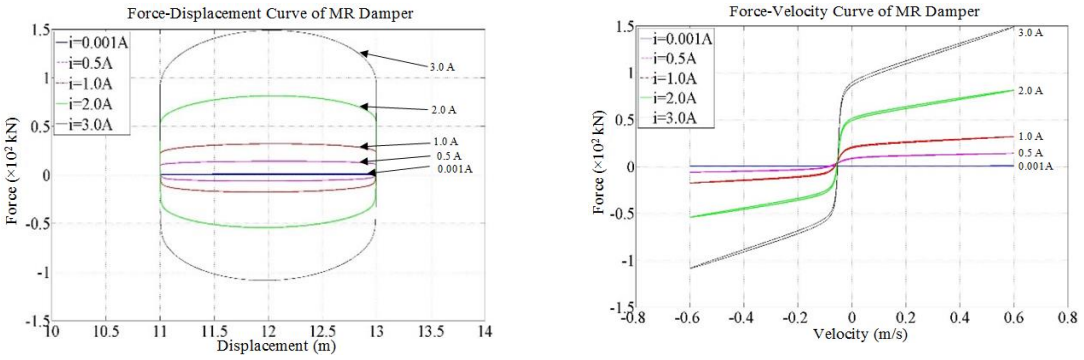

(a) (b)

Fig. 14 Variation of damping force at primary MR damper with input currents, (a) force-displacement curves, and (b) force-velocity curves; with sinusoidal excitation amplitude = 1.0 m and sinusoidal excitation frequency = 0.6 rad/s, initial piston position offset = +12.0 m (+39.37 ft)

4. Numerical analyses on suppression of HPT tension variations

In the developed dynamic coupling of tension-variation suppression by MR damper into the conventional hydro-pneumatic tensioner (HPT), the additional effect of dynamic tension variations by viscous fluids (Kang *et al.* 2017) is implemented. The host platform in this numerical analysis is a generic type tension-leg platform (TLP) as shown in Fig. 15 (Yang 2009).

The principal dimensions and load conditions of the TLP platform are tabulated in Table 3 (Kim *et al.* 2001, Yang 2009). The finite-element equations for the high-order line members are coupled with the TLP platform dynamics by using the linear and rotational spring and dashpot (Garrett 1982) for the eight tendons, hydro-pneumatic riser tensioner (Yang and Kim 2010) for the seven production and one drilling TTRs, as listed in Table 4. The MR dampers, with the capacity up to ~150 kN as proposed in Table 2, work corporately with the drilling riser as conceptually illustrated in the Fig. 8(a). The hull-riser-tendon coupled analyses for EFCC are conducted in the following settings, (i) TLP under regular wave input; and (ii) TLP under irregular-sea condition, as tabulated in Table 5.

4.1 Suppression of HPT tension variations under regular wave

The simulated dynamic responses of the hydro-pneumatic (HP) tensioner with TLP platform are shown in Fig. 16(a). The HPT was excited by a sinusoidal wave-loading input. The position of tensioner ring (TR) after achieving the steady-state is at around -17.0 ft (-5.18 m) (negative sign refers to that the tensioner ring is traveling back-and-forth in the range below the initial mid-point position which is at 0 ft (0 m)). The dynamic displacement is from -16.1 ft (-4.91 m) to -17.7 ft (-5.39 m) and the velocity of tensioner ring is from ~ -0.125 ft/s (~ -0.038 m/s) to ~0.175 ft/s (~0.053 m/s). It can be found that the displacement and velocity are out of phase, with the maximum velocities occurring as the tensioner ring reaches its steady-state equilibrium position at ~ -17.0 ft (~ -5.18 m). It is noteworthy that the velocity of the tensioner ring is far below 1.0 ft/s (0.305 m/s) in the TLP since the platform heave motion is constrained by the highly stiffed tendons.

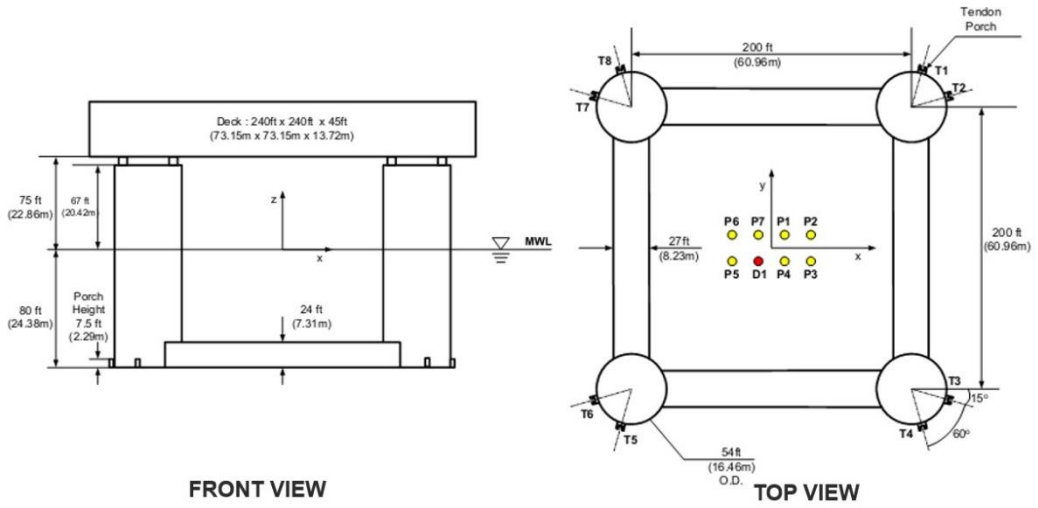

Fig. 15 Layout of TLP model (Yang 2009)

Table 3 Principal dimensions and load conditions of the generic TLP model

Water depth	914.36 m
Number of column	4
Column cross-sectional diameter	16.45 m
Column center-to-center distance	60.96 m
Column freeboard	20.42 m
Pontoon breadth	8.23 m
Pontoon height	7.31 m
Height of deck bottom from mean water level (MWL)	22.86 m
Deck height	12.19 m
Draft	24.38 m
Vertical distance from center of gravity to MWL	8.56 m
Vertical distance from center of buoyancy to MWL	-15.18 m
Distance from center of pressure to MWL	38.10 m
Roll radius of gyration	33.19 m
Pitch radius of gyration	33.19 m
Yaw radius of gyration	32.40 m
Wind load coefficient	3.18 kN/(m/s)^2
Total weight	24,157 MT
Tendon pretension at the top	7,040 MT
Riser pretension at the top	1,972 MT
Displacement	32,775 MT

In this TLP case, the static equilibrium tension is around 572 kips (2544 kN), which is lower than the total pretension as listed in Table 4 because the total weights, payloads, and offset effects have been considered in this static equilibrium tension. The dynamic tension variations (from ~569 kips (~2531 kN) to ~576 kips (~2562 kN)) are mainly caused by the changing ratio of gas volume, which can be referred to $\Delta z/z_{A0}$ with uniform cross-sectional area, as stated in the Eq. (2). It can be found that the dynamic tension variations in the TLP case are minor because the velocity of the tensioner ring is very small.

The EFCC is proposed to further reduce the variations of dynamic tension. The effect of the EFCC scheme on the dynamic tension is shown in Fig. 16(b) and the tension-stroke curve is shown in Fig. 17. In this simulation case, the dynamic tension can be suppressed as much as 88% (tension variation was reduced from ~7 kips (~31.14 kN) to less than 1 kips (4.45 kN)) by using the EFCC scheme. The tension-stroke curve for the simulation starts from the initial state to the steady-state as shown in Fig. 17(a). The EFCC was activated at a threshold value z_T = -14.20 ft (-4.33 m) in this case. The MR dampers with constant force actuators (CFA), as conceptually illustrated in Fig. 8(a), act as a force compensator. Since the EFCC scheme is proposed for precise tension control, it will be activated only under the situation when the axial tension variation must be controlled within very strict limits, such as during the offshore drilling. Therefore, a practical EFCC system can be designed as a separated module that can be mounted/dismounted on the conventional HP tensioner.

Table 4 Configurations of the tendons and TTRs in TLP model

	Top-end Coordinate			Bottom-end Coordinate			
	X (m)	Y (m)	Z (m)	X (m)	Y (m)	Z (m)	T_o (MT)
T1	33.01	39.90	-22.10	33.01	39.90	-921.26	880.0
T2	39.90	33.01	-22.10	39.90	33.01	-921.26	880.0
T3	39.90	-33.01	-22.10	39.90	-33.01	-921.26	880.0
T4	33.01	-39.90	-22.10	33.01	-39.90	-921.26	880.0
T5	-33.01	-39.90	-22.10	-33.01	-39.90	-921.26	880.0
T6	-39.90	-33.01	-22.10	-39.90	-33.01	-921.26	880.0
T7	-39.90	33.01	-22.10	-39.90	33.01	-921.26	880.0
T8	-33.01	39.90	-22.10	-33.01	39.90	-921.26	880.0
D1	-2.29	-2.29	0.00	-2.29	-2.29	-914.36	330.7
P1	2.29	2.29	0.00	2.29	2.29	-914.36	234.5
P2	6.86	2.29	0.00	6.86	2.29	-914.36	234.5
P3	6.86	-2.29	0.00	6.86	-2.29	-914.36	234.5
P4	2.29	-2.29	0.00	2.29	-2.29	-914.36	234.5
P5	-6.86	-2.29	0.00	-6.86	-2.29	-914.36	234.5
P6	-6.86	2.29	0.00	-6.86	2.29	-914.36	234.5
P7	-2.29	2.29	0.00	-2.29	2.29	-914.36	234.5

* T = tendon; D = drilling riser; P = production riser

Table 5 Wave, current, and wind profiles of the central-Gulf of Mexico (GOM) 100-year condition

Significant wave height, H_s		15.8 m
Peak period, T_p		15.4 s
Overshooting parameter, γ		2.40
Direction of waves and current (collinear)		0 deg
Current profile	Surface speed	2.41 m/s
	Speed at mid-profile	1.80 m/s
	Zero-speed depth	100.80 m
Wind	10 m elevation	48.00 m/s

The required force F_{req} and combined MR damper forces ($F_{MR}{}^{P}$+$F_{MR}{}^{S}$) in time series after the EFCC was activated are shown in Fig. 18. A certain range from 1170 sec to 1250 sec is magnified in Fig. 18(b). It can be found that the combined MR damper (MRD) forces F_{MR} from the primary MRD and secondary MRD matched with the required force F_{req} with the deviation less than 2%. The combined MRD force is acting in the opposite direction of actuator force in order to fine-tune the net force to be transferred to the tensioner ring. As shown in Fig. 18(b), the primary MRD is the

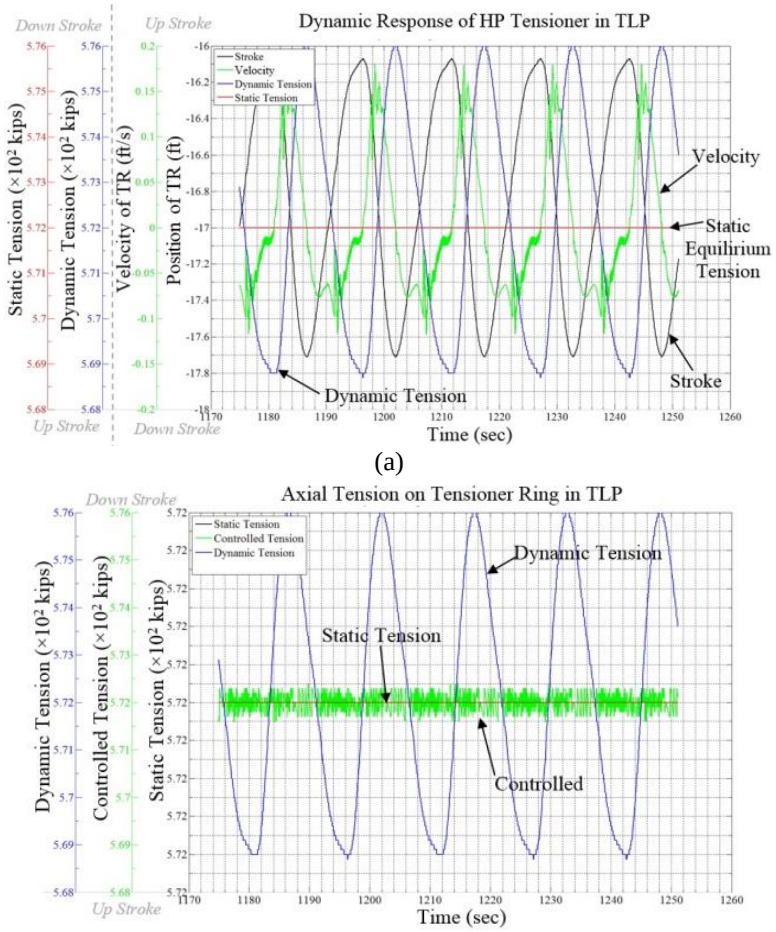

Fig. 16 (a) Dynamic response of HP tensioner and (b) Axial tension on tensioner ring, for simulation time-step from 1174 sec – 1251 sec

predominant resistive force provider while the secondary MRD is activated only if the limitation of primary MRD is encountered. The combined MRD force is a trade-off between the tensioner properties, the capacity of the selected MR dampers, the targeting tension, and the characteristics of force actuator. Hence, the combined damping force must be determined for different applications with respect to the appropriate operational limits of MR damper.

4.2 Suppression of HPT tension variations under sea condition

The dynamic responses of the HPT in TLP under irregular-sea condition, representing GOM 100-yr storm as stated in Table 5, are shown in Fig. 19. In the simulation time step from 4520 s to 4660 s (in Fig. 19(a)), the position of tensioner ring (TR) was traveling in the range from -16.00 ft (-4.88 m) to -12.25 ft (-3.73 m) and the velocity of tensioner ring was from ~ -0.210 ft/s (~ -0.064 m/s) to ~0.175 ft/s (~0.053 m/s). It can be found that the position and velocity of the tensioner ring were out

of phase i.e. the velocities reach zero when the tensioner ring reaches its local maxima. The velocity of the tensioner ring is far below 1.0 ft/s (0.305 m/s) in the TLP since the heave motion of TLP is constrained by the highly stiffed tendons.

The dynamic tension variations in this particular case were varying from ~551 kips (~2450 kN) to ~569 kips (~2531 kN). The effect of EFCC scheme on the dynamic tension is shown in Fig. 19(b) and the tension-stroke curves are shown in Fig. 20. In this case, the dynamic tension variations can be suppressed as much as 94%, where the tension variations were reduced from ~18 kips (~80 kN) to less than 1 kips (4.45 kN) by using the EFCC scheme.

The tension-stroke curve for the simulation started from the initial state to the steady-state is shown in Fig. 20(a). The required force F_{req} and combined MR damper forces ($F_{MR}{}^{P}+F_{MR}{}^{S}$) after the EFCC was activated are shown in Fig. 21. A certain range of 4520 s to 4660 s is magnified in Fig. 21(b). The combined MRD force from primary MRD and secondary MRD matched with the required force F_{req} with the deviation less than 2%.

The force actuator can be either the pneumatic/hydraulic actuator or any other type with which output force is not required to be in very high precision. The accuracy of net tension acting on the tensioner ring is fully adjustable by the MR dampers. The reduction of tension variations can be achieved cost-effectively by this method, as an alternative to the expensive high-precision active force compensator. Moreover, the capacity for very large compensated force outputs, especially in the offshore applications, is not readily available for precision active force actuators. The MR damper has the advantage to react very fast and therefore it is appropriate to be used in the EFCC. It is noteworthy that the addition of linear actuator may not be practical in the long-term application but it can be implemented in the short-term application when the tension of riser must be maintained strictly, for instance during the drilling operation. The dimension of the MR dampers and force actuators are assumed ideally here to be commensurate with the size of the tensioner. The optimization of the equipment sizing, redundancy, and layout are not in the scope of the current study and can be conducted in the future work.

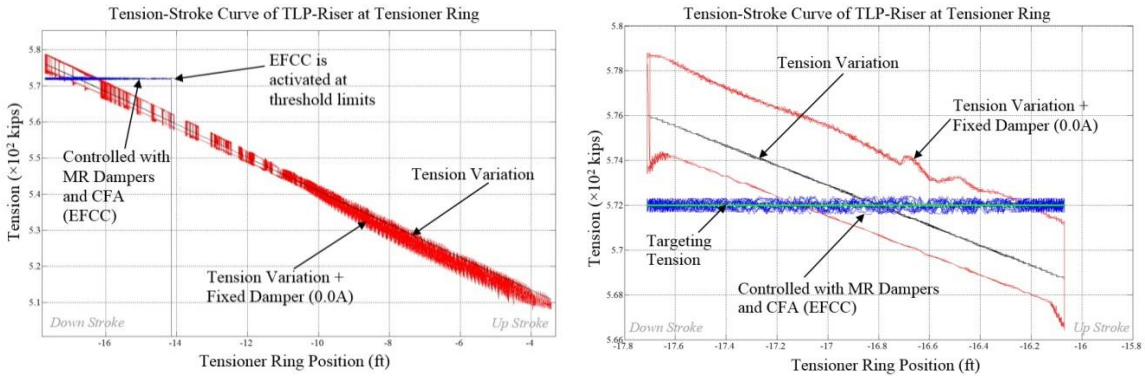

Fig. 17 Tension-stroke curve of TLP-riser at the tensioner ring (TR) under steady-state, (a) from initial condition of simulation; (b) for the TR's position range from ~-4.89 m to ~ -5.39 m

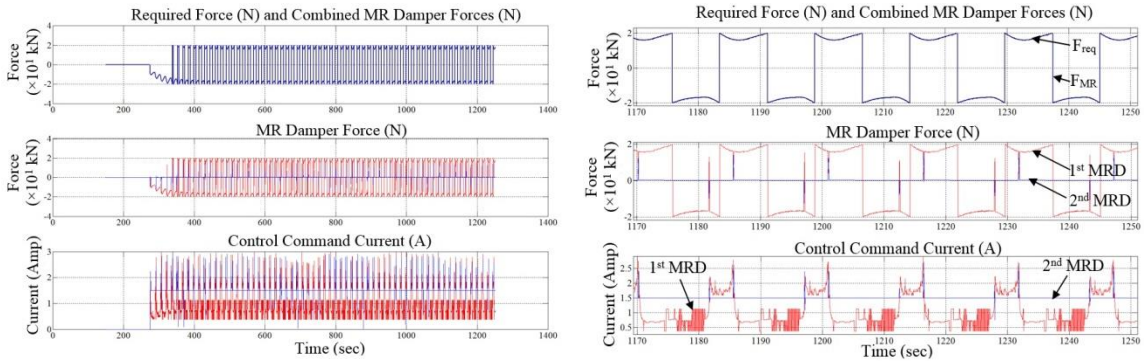

(a) (b)

Fig. 18 Controlled force outputs and control current, (a) from initial condition of simulation and (b) for the range from 1170 sec to 1250 sec

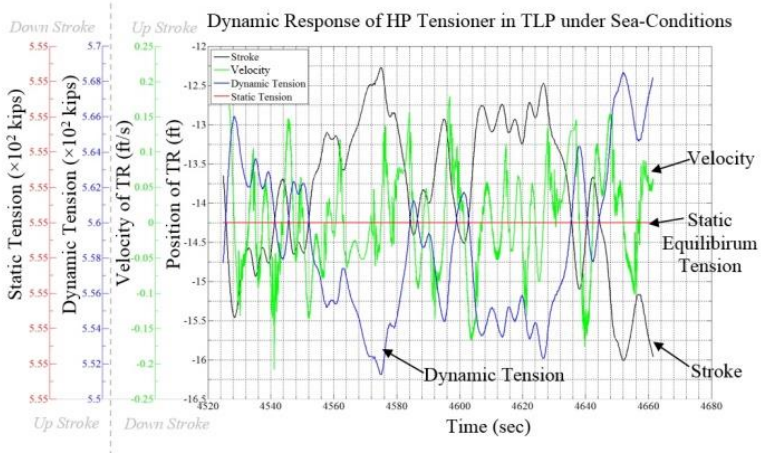

(a)

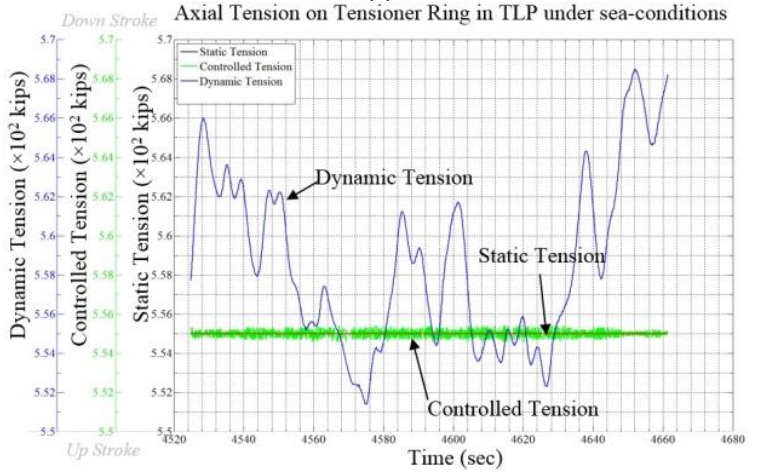

(b)

Fig. 19 (a) Dynamic response of HPT, and (b) axial tension on tensioner ring, under irregular wave for simulation time-step from 4520 sec – 4660 sec

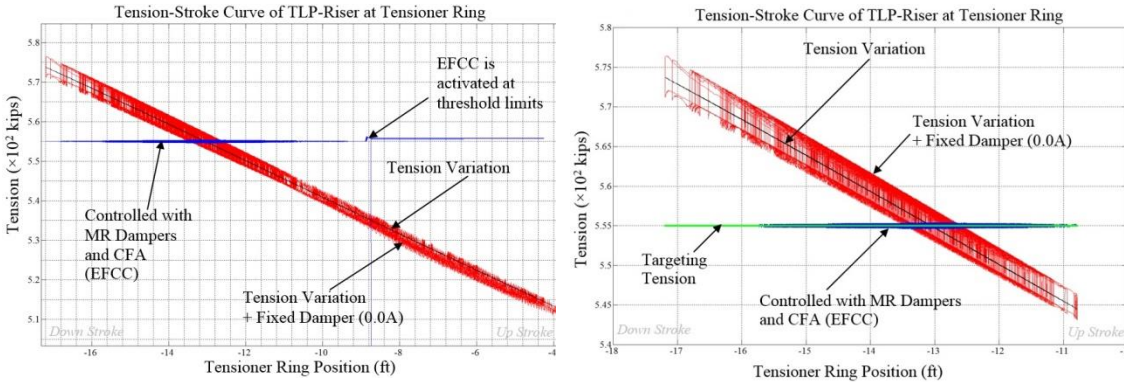

(a) (b)

Fig. 20 Tension-stroke curve of TLP-riser at the tensioner ring (TR) under irregular wave, (a) from initial condition of simulation and (b) for the TR's position range from ~ -4.89 m to ~ -5.39 m

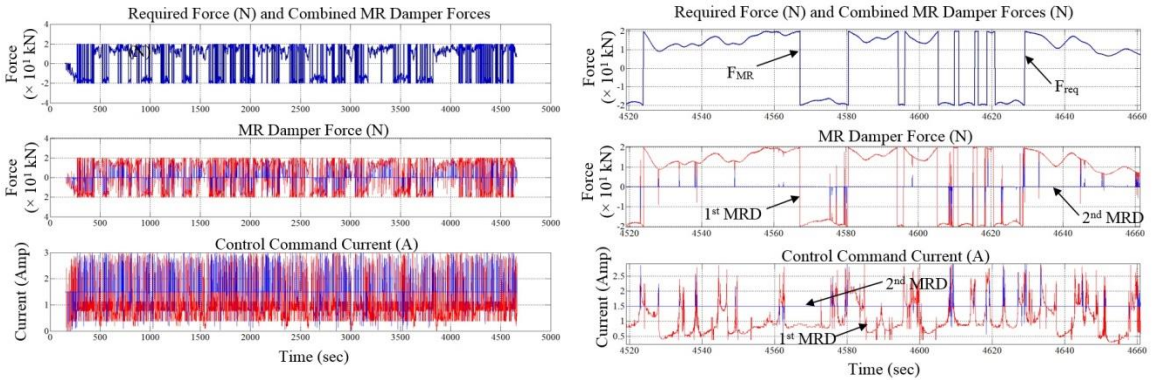

(a) (b)

Fig. 21 Controlled force outputs and control current, (a) from initial condition of simulation and (b) for the range from 4520 sec to 4660 sec, under the sea conditions

5. Conclusions

In this paper, a method for suppressing the tension variations in hydro-pneumatic riser tensioner was developed by using MR damper and force actuator. The dynamic tension variations in the conventional HPT can significantly be larger when considering the friction of viscous fluid and its effect is adequately modeled. The damping force of MR damper increases with the increment of command current i, excitation amplitude A, and excitation frequency ω, and it approaches a limiting value when the electric current gets a certain value. The MR damper is also sensitive to the initial piston position where it displays symmetry characteristic in the force-displacement loop when pretension is applied. The combined MR damper force is a trade-off between the tensioner properties, the capacity of the selected MR dampers, the targeting tension, and the characteristics of force actuator. The MR damper is formulated by using Nonlinear Hysteretic Arctangent Function (NHAF) model.

The integration of MR damper into the HPT mathematical model was accomplished. The targeting MR damper force F_{MR} can be iterated until its deviation from the required force F_{req} is less than two-percent.

The Equivalent Force Compensation Control (EFCC) was able to reduce the tension variations between the actual TTR tension and the desired tension by using a combination of MR dampers and force actuators. In the simulation, the EFCC scheme can suppress the dynamic tension variations as much as 88% under the regular wave condition and 94% under the 100-yr-storm irregular-sea condition. The EFCC scheme was proposed for precise tension control that can be activated only under the situation, in which the axial tension variation must be controlled within very strict limits, such as during the offshore drilling.

Acknowledgments

The authors would like to appreciate Sabah Shell Petroleum Co. Ltd. for the financial support in preparing this paper.

References

Bae, Y.H. and Kim, M.H. (2013), "Influence of failed blade-pitch-control system to FOWT by aero-elastic-control-floater-mooring coupled dynamic analysis", *Ocean Syst. Eng.*, **3**(4), 295-307.

Dominguez, A., Sedaghati, R. and Stiharu, I. (2008), "Modeling and application of MR dampers in semi-adaptive structures", *Comput*. Struct., **86** (3-5), 407-415.

Duan, Y.F., Ko, J.M., Ni, Y.Q. and Chen, Z.Q. (2002), "Field comparative tests of cable vibration control using magnetorheological (MR) dampers in single-and twin-damper setups", *Proceedings of the 3rd Int. Conference on Advances in Steel Structures*, Hong Kong, China, December.

Friedman, A.J. and Shirley, J.D. (2012), "Development and experimental validation of a new control strategy considering device dynamics for large-scale MR dampers using real-time hybrid simulation", Technical report, Intelligent Infrastructure Systems Lab Technical Report IISL-003, Purdue University, West Lafayette, USA.

Gallagher, C., Williams, D. and Lang, D. (2012), "Modelling of marine riser tensioner load variations and implications for minimum top tension settings in drilling risers", *Proceedings of the 31st International Conference on Ocean, Offshore and Arctic Engineering*, Rio de Janeiro, Brazil, June.

Garrett, D.L. (1982), "Dynamic analysis of slender rods", *Energy Resour. Technol.*, **104**(4), 302-306.

Grønevik, A. (2013), "Simulation of drilling riser disconnection - recoil analysis", M.Sc. Thesis, Norwegian University of Science and Technology, Trondheim.

Hurlebaus, S. and Gaul, L. (2006), "Review: Smart structure dynamics", *Mech. Syst. Signal Pr.*, **20**(2), 255-281.

Kang, H.S. (2015), "Semi-active magneto-rheological damper and applications in tension leg platform / semi-submersible", Ph.D. Dissertation, Texas A&M University, College Station, USA.

Kang, H.S., Kim, M.H., Bhat Aramanadka, S.S. and Kang, H.Y. (2013), "Semi-active magneto-rheological damper to reduce the dynamic response of top-tension risers", *Proceedings of the 23rd International Offshore and Polar Engineering Conference*, Anchorage, USA, June.

Kang, H.S., Kim, M.H., Bhat Aramanadka, S.S. and Kang, H.Y. (2014), "Dynamic response control of top-tension risers by a variable damping and stiffness system with magneto-rheological damper", *Proceedings of the 33rd International Conference on Ocean, Offshore and Arctic Engineering*, San Francisco, USA, June.

Kang, H.S., Kim, M.H. and Bhat Aramanadka, S.S. (2017), "Tension variations of hydro-pneumatic riser

tensioner and implications for dry-tree interface in semisubmersible", *Ocean Syst. Eng.*, **7**(1), 21-38.
Kang, H.Y. and Kim, M.H. (2012), "Hydrodynamic interactions and coupled dynamics between a container ship and multiple mobile harbors", *Ocean Syst. Eng.*, **2**(3), 217-228.
Kim, M.H., Tahar, A. and Kim, Y.B. (2001), "Variability of TLP motion analysis against various design methodologies/parameters", *Proceedings of the 11th International Offshore and Polar Engineering Conference*, Stavanger, Norway, USA, June.
Kim, Y. (2007), "Nonlinear identification and control of building structures equipped with magnetorheological dampers", Ph.D. Dissertation, Texas A&M University, College Station.
Kim, S.J. and Kim, M.H. (2015), "Dynamic behaviors of conventional SCR and lazy-wave SCR for FPSOs in deep water", *Ocean Eng.*, 106, 396-414.
Koo, B.J., Kim, M.H. and Randall, R. (2004), "The effects of nonlinear multi-contact coupling with gap between risers and guide frame on global spar motion analysis", *Ocean Eng.*, **31**(11-12), 1469-1502.
Kozik, T.J. (1975), "An analysis of a riser joint tensioner system", *Proceedings of the Offshore Technology Conference*, Houston, USA, May.
Kozik, T.J. and Noerager, J. (1976), "Riser tensioner force variations", *Proceedings of the Offshore Technology Conference*, Houston, USA, May.
Lee, C.H. and Newman, J.N. (1991), "First-and second-order wave effects on a submerged spheroid", *Ship Res.*, **35**(3), 183-190.
Li, S., Campbell, M., Howells, H. and Orsak, J. (2013), "Tension loss of hydro-pneumatic riser tensioners", *Proceedings of the 32nd International Conference on Ocean, Offshore and Arctic Engineering*, Nantes, France, June.
Ozbulut, O.E., Bitaraf, M. and Hurlebaus, S. (2011), "Adaptive control of base-isolated structures against near-field earthquakes using variable friction dampers", *Eng. Struct.*, **33**(12), 3143-3154.
Ran, Z. (2000), "Coupled dynamic analysis of floating structures in waves and currents", Ph.D. Dissertation, Texas A&M University, College Station, USA.
Spencer Jr, B.F., Dyke, S.J., Sain, M.K. and Carlson, J.D. (1997), "Phenomenological model for magnetorheological dampers", *Eng. Mech.*, **123**(3), 230-238.
Sten, R., Hansen, M.R., Larsen, C.M. and Sævik, S. (2010), "Force variations on heave compensating system for ultra-deepwater drilling risers", *Proceedings of the 29th International Conference on Ocean, Offshore and Arctic Engineering*, Shanghai, China, June.
Trent, D. (2012), "Tensioner system with recoil controls", *U.S. Patent*: 8,157,013 B1, issued Apr. 17, 2012.
Tse, T. and Chang, C.C. (2002), "Seismic protection of base-isolated structures using semi-active MR dampers", *Adv. Build. Technol.*, **1**, 529-536.
Yang, G., Spencer Jr, B.F., Jung, H.J. and Carlson, J.D. (2004), "Dynamic modeling of large-scale magnetorheological damper systems for civil engineering applications", *Eng. Mech.*, **130**(9), 1107-1114.
Yang, C.K. (2009), "Numerical modeling of nonlinear coupling between lines/beams with multiple floating bodies", Ph.D. Dissertation, Texas A&M University, College Station.
Yang, C.K. and Kim, M.H. (2010), "Linear and nonlinear approach of hydropneumatic tensioner modeling for Spar global performance", *Offshore Mech. Artic Eng.*, **132**(1), 011601.
Yang, C.K. and Kim, M.H. (2011), "The structural safety assessment of a tie-down system on a tension leg platform during hurricane events", *Ocean Syst. Eng.*, **1**(4), 263-283.
Yang, M.G., Chen, Z.Q. and Hua, X.G. (2011), "An experimental study on using MR damper to mitigate longitudinal seismic response of a suspension bridge", *Soil Dynam. Earthq. Eng.*, **31**(8), 1171-1181.
Yao, G., Yap, F., Chen, G., Li, W. and Yeo, S. (2002), "MR damper and its application for semi-active control of vehicle suspension system", *Mechatronics*, **12**(7), 963-973.